Optimal transceiver placement and resource allocation schemes in cooperative dynamic FSO networks

ABDALLAH S. GHAZY,[1] **MAHMOUD A. HASABELNABY,**[2,*] **HOSSAM A. I. SELMY,**[3] **AND HOSSAM M. H. SHALABY**[4]

[1]*Department of Electronics and Communications Engineering, McMaster University, Ontario L8S 4L8, Canada*
[2]*Faculty of Electronic Engineering, Menoufia University, Menouf, Egypt*
[3]*National Institute of Laser Enhanced Science (NILES), Cairo University, Egypt*
[4]*Faculty of Engineering, Alexandria University, Alexandria, Egypt*
Corresponding author: mahmoud.hasabelnaby@el-eng.menofia.edu.eg

Cooperative dynamic free-space optical (FSO) networks exploit the fact that atmospheric losses are distance dependent to enhance the performance of FSO networks. This enhancement is achieved by sharing the resources of shorter links among different nodes in the network. In this paper, two joint transceiver placement and resource allocation schemes are proposed to optimally place FSO redundant transceivers based on optimal resource allocation in cooperative dynamic FSO networks. Specifically, one scheme increases reliability and capacity, while the other increases reliability and fairness of cooperative dynamic FSO networks during severe weather conditions. The schemes are formulated as multi-objective and bi-level integer linear programming problems and solved using an exhaustive search to obtain optimal solutions. The numerical results reveal that higher reliabilities can be achieved with enhanced capacities and fairness using the first and second schemes, respectively. Furthermore, these improvements are achieved by using many fewer numbers of FSO redundant transceivers than those of random placement.   © 2019 Optical Society of America

https://doi.org/10.1364/JOCN.11.000512

1. INTRODUCTION

A free-space optical (FSO) link can provide transmission of several gigabytes over a few kilometers distance. FSO presents a promising solution for the last-mile connectivity problem, where several remote nodes have to be connected to a center backbone node. This is because of its multiple advantages such as wide bandwidth, high security, cost effectiveness, and flexible networks. Figure 1 shows one possible application for FSO links [1,2]. Regardless of the attractive features of FSO, it suffers from free-space channel impairments in the infrared (IR) band spectrum, i.e., weather conditions, background radiation, air turbulence, and eye safety regulations [1,3,4]. The weather conditions include fog, rain, snow, and dust that could absorb and scatter the transmitted optical signal [5].

Generally, FSO networks need topology control schemes that focus on how nodes communicate with the backbone node and to overcome the interruption of FSO links [6]. Practically, there are several challenges that complicate the operation of FSO topology control schemes. Mainly, due to the implementation cost, there is a limited number of deployed FSO transceivers that can affect the connectivity of the FSO network. Also, FSO links have small transmission distances, so many hops are needed to enlarge the service area [7].

A better performance of FSO networks can be obtained in various weather conditions by implementing dynamic configuration management, where the traffic of each node can be rerouted to intermediate nodes in order to reach the backbone node. Recently, the development of pointing, acquisition, and tracking (PAT) systems has made dynamic (reconfigurable) FSO networks more feasible than before [8]. In cooperative dynamic FSO networks, nodes share their optical resources (transmission rates) to keep connectivities between the backbone node and far nodes even in severe weather conditions. As shown in Figs. 1 and 2, the links are reconfigured so that near nodes act as virtual relays to survive far nodes in severe weather conditions. Therefore, real-time monitoring and management are important in mobile FSO networks in order to ensure the network is operated effectively.

A. Related Work

Suitable FSO network topologies have been investigated to mitigate severe weather conditions and provide the required
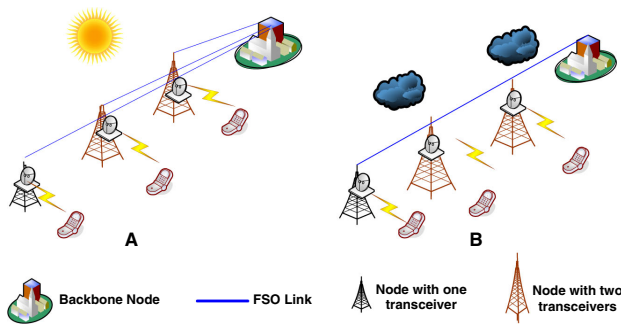
Fig. 1. Typical wireless application for cooperative reconfigurable FSO links in last-mile network. (A) In clear weather. (B) In foggy weather.
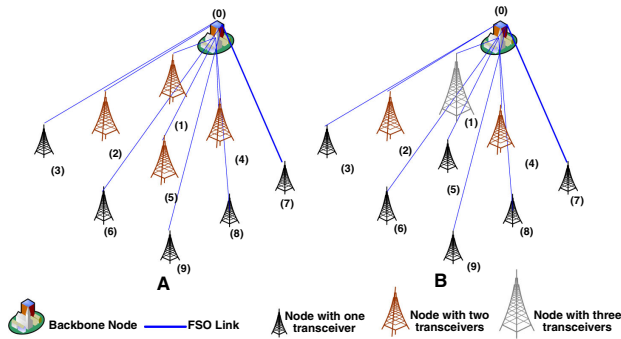
Fig. 2. Two forms for transceiver distribution. (A) Outer nodes are equipped by one transceiver, while inner nodes are equipped by two transceivers. (B) Outer nodes are equipped by one transceiver, while inner nodes are equipped by one, two, or three transceivers.

quality of service (QoS) for different nodes. Specifically, serial-relayed topology has been addressed, where multi-hop FSO transmission takes advantage of the resulting shorter hops [5,9]. Also, due to the resultant backup links, more robust static FSO networks can be realized by implementing mesh topologies [10,11]. Toward further improvements in the performance of these FSO networks, optimal placement of relay nodes in multi-hop networks and the number of transceivers used in each node in mesh networks have been investigated [12–15]. However, to enhance the reliability of these static topologies, large numbers of redundant FSO transceivers have to be installed, which results in higher implementation costs.

Through using improved PAT systems, better performances have been demonstrated at much lower costs for cooperative and non-cooperative dynamic FSO networks [16–18]. Efficient resource allocation schemes have recently been proposed to fairly allocate network resources among different FSO nodes for certain FSO transceiver distribution in cooperative dynamic FSO networks [17,19–21]. In non-cooperative dynamic FSO networks, transmission rates of virtual relays are not shared, and hence their link capacities are increased to allow transmission of switched traffic [16].

Generally, to enable network reconfiguration, additional FSO transceivers are installed on the inner nodes of the network. However, the placement of these additional transceivers on the inner nodes plays an important role in network

performance [22]. For a given number of these additional transceivers, many feasible transceiver placements can be realized, as indicated in Fig. 2. Recently, optimal transceiver placement and resource allocation schemes have been introduced to enhance the reliability and fairness of dynamic cooperative FSO networks [23–25]. These schemes exploit the fact that cooperative dynamic FSO networks can be continually reconfigured to the optimal topologies (configurations) that yield the best performance in given weather conditions. Furthermore, FSO links could be added to other radio frequency (RF) and visible light communication (VLC) systems to enhance network performance. In [26,27], the performance of multi-hop hybrid FSO/RF networks is studied using hybrid automatic repeat request (HARQ). Efficient transceiver placement and resource allocation schemes are proposed for hybrid FSO/RF networks in order to enhance network performance, especially in severe weather conditions [28–31]. In Refs. [32,33], a hybrid FSO/VLC system is proposed as a solution to overcome the last-mile and last-meter access networks bandwidth bottleneck.

B. Contributions

In this paper, two joint optimal transceiver and resource allocation schemes are proposed for cooperative dynamic FSO networks. The schemes aim to optimally place the FSO transceivers among different nodes and then allocate network resources to maximize network performance. Particularly, the paper has the following contributions:

• Given the number of FSO transceivers installed in the network as a cost constraint and the geographical distribution of nodes in the service area along with possibilities of line-of-sight (LOS) connectivity among them, the optimal transceiver placement is obtained once forever, based on the annual weather distribution in the service area.

• Once the optimal placement of FSO links is deployed, real-time optimal resource allocation is performed in various weather conditions to achieve the best performance.

• The proposed schemes are formulated as multi-objective and multilevel optimizations, where different prioritized objectives—namely, network reliability, capacity, fairness, average transmitted power, and average bit error rate (BER)—are targeted.

• The first proposed scheme prioritizes reliability as the highest priority objective (essential objective of the dynamic FSO network), then capacity, average transmitted power, and average error rate in descending optimization order. In contrast, toward achieving higher reliability and fairness levels in the network, the second scheme replaces the capacity objective with the fairness objective.

• The proposed joint optimizations are carried out in two steps. In the first step, optimal resource allocations are evaluated for each feasible transceiver placement. In the second step, the optimal transceiver placement is obtained by selecting from all feasible placements the one that gives the highest annual average performance.

• The resource allocation optimizations are modified versions of the ones proposed in [17]. The modification is

carried out by adding the objective of minimizing the number of dropped nodes to the optimization.

- The impacts of transmission rate and transmitted power adaptations for FSO links on network performance are investigated.
- The performances of the proposed schemes are evaluated in foggy weather conditions. The numerical results reveal that the proposed schemes achieve better average network reliability and bit rate fairness/capacity performance compared to random placements.
- The degradation in network performance caused by non-optimal transceiver placement is also illustrated.

The rest of this paper is organized as follows. In Section 2, a FSO link model is illustrated. In Section 3, FSO placement vector parameters are described. Section 4 is devoted to the formulation of optimization problems of the proposed schemes. In Section 5, the schemes' complexity is discussed and computed. Numerical evaluations of the proposed schemes are presented in Section 6. Finally, the conclusions and remarks are given in Section 7.

2. FSO LINK MODEL

Two main factors affect FSO link performance, namely, link losses and noises. Link losses include both atmospheric and geometric losses. Obviously, the air scattering, absorption, and beam spreading result in link losses. The system noises include background noise that comes from external radiation sources along with dark current and thermal noises that are generated from internal components of the optical receiver [34–36].

Many natural phenomena degrade the quality of optical signal in the atmosphere such as fog, rain, and snow events. The fog loss γ_{fog}, such as haze, low clouds, dust, and smoky weather conditions, is defined by several empirical models. For low visibility ($V < 6$ km) FSO links, the Kim model is the most accurate [1]:

$$\gamma_{\text{fog}} = 10 \log(\exp[Q \times L]) \ \text{dB}, \tag{1}$$

where L is the distance in km, and Q is the total extinction coefficient, given by

$$Q = \frac{3.91}{V} \times (\lambda/550)^{-\Psi}. \tag{2}$$

Here, V is the visibility in km, λ is the wavelength in nm, and Ψ is the distribution of scattering particle size, given by

$$\Psi = \begin{cases} 1.6; & V > 50, \\ 1.3; & 6 < V < 50, \\ 0.16V + 0.34; & 1 < V < 6, \\ V - 0.5; & 0.5 < V < 1, \\ 0; & V < 0.5, \end{cases} \tag{3}$$

where V is in km. In rainy weather, the attenuation is caused by optical scattering due to droplets of water. The rain loss is calculated using Japan's empirical model [4]:

$$\gamma_{\text{rain}} = 1.58 \times D^{0.63} \times L \ \text{dB}, \tag{4}$$

where D is the rain fall rate in mm/h. In snowy weather, the attenuation is wavelength sensitive, but the sensitivity is not

significant, i.e., the loss is approximately equal in a wide range of wavelengths. The models for both wet (γ_{snow_w}) and dry (γ_{snow_d}) snow losses are given by [4]

$$\gamma_{\text{snow}_w} = (1.02 \times 10^{-4}\lambda + 3.79) \times S_w^{0.72} \times L \ \text{dB},$$

$$\gamma_{\text{snow}_d} = (5.42 \times 10^{-5}\lambda + 5.50) \times S_d^{1.38} \times L \ \text{dB}, \tag{5}$$

respectively, where S_w and S_d are the wet and dry snow fall rates in mm/h, respectively. Even in clear weather conditions, geometric loss is present due to optical beam spreading through the propagation in free space. This loss is calculated by [3]

$$\gamma_{\text{geo}} = 10 \times \log \left(\frac{d_t + L \times \Theta}{d_r} \right)^2 \ \text{dB}, \tag{6}$$

where d_r is the receiver diameter in mm, d_t is the transmitter diameter in mm, and Θ is divergence angle in mm · rad/km.

In this paper, the receiver diameter is assumed to be large enough, so that the impact of weak turbulence is small, and during severe weather conditions, the scintillation loss is relatively small and can be neglected [5,37]. In this case, the total FSO link equation is given as [38]

$$P_r = P_t \times E_t \times E_r \times 10^{\left(\frac{-\gamma}{10}\right)}, \tag{7}$$

where P_r is the recieved power, P_t is the transmitted power, L is the link length, E_t is the transmitter optical efficiency, E_r is the receiver optical efficiency, and γ is total FSO link loss given by [39]

$$\gamma = \gamma_{\text{fog}} + \gamma_{\text{rain}} + \gamma_{\text{snow}_w} + \gamma_{\text{snow}_d} + \gamma_{\text{geo}}. \tag{8}$$

It is remarkable that fog and rain rarely occur concurrently in nature [40]. However, it can rain and snow simultaneously, especially in the transition period during which snow is changing to rain or rain is changing to snow [41,42]. Therefore, in foggy weather, $\gamma = \gamma_{\text{fog}} + \gamma_{\text{geo.}}$, while in rainy and snowy weather, $\gamma = \gamma_{\text{rain}} + \gamma_{\text{snow}} + \gamma_{\text{geo.}}$ [39].

In order to overcome these losses and maintain network performance, FSO links could operate with variable transmitted power and bit rate levels [43]. Obviously, in clear weather conditions, the highest transmission rate with an acceptable error rate is achieved by transmitting the lowest average power level. In contrast, during bad weather conditions, the average BER is maintained by increasing the level of transmitted power and/or reducing the link transmission rate. However, the maximum average transmitted power is restricted by eye safety regulations [1,3,4].

When the background radiation level is relatively high, the receiver thermal noise can be ignored, and the system noise is modeled as a Poisson shot-noise-limited receiver. The prime of the intensity modulation-direct detection (IM-DD), non-return-to-zero on–off keying (NR-OOK) technique is used in our performance evaluations [44]. Furthermore, in the considered geographical area, homogeneous weather is assumed, i.e., all FSO links are affected by the same specific atmospheric losses (dB/km) and background radiation levels. Clearly, this assumption is valid as long as the coverage area is relatively small.

3. TRANSCEIVER PLACEMENT PARAMETERS IN COOPERATIVE DYNAMIC FSO NETWORKS

In the considered cooperative dynamic FSO networks, under clear weather conditions, all nodes are directly connected to the central node for fair resource access, as indicated in Fig. 1(A). However, in severe weather conditions, far nodes could switch their direct links to other near nodes to maintain connectivity to the central node, as indicated in Fig. 1(B). Particularly, in fair cooperation, the node with a bad direct link switches its traffic to a node with a better link, and the transmission rate of the shared link is divided fairly. However, in reliable cooperation, the node switches its traffic only in the case that the direct link is dropped, and the minimum transmission rate is offered. Clearly, in order to increase the number of alternative paths from/to a node, the number of installed transceivers at this node must be increased, as indicated in Fig. 2. However, a large number of redundant optical transceivers results in rising network cost, probability of misalignment, and link interference. Consequentially, efficient placement of FSO transceivers in FSO nodes is an essential issue in order to increase network performance and reduce implementation cost.

Generally, the cooperative FSO network consists of N nodes $(v_1, \ldots, v_N)$ with arbitrary geographical distribution in addition to the backbone node v_0. The geographical distribution of FSO nodes is obtained from traffic maps and radio planning in the given service area. However, because FSO is a LOS technology [1], the existing infrastructure and geographical topology in the service area could prevent the establishment of LOS connections between some nodes. The LOS status between all nodes in the network is given by $(N+1) \times (N+1) \Phi = [\Phi_{i,j}]$ matrix of binary indicators, where $\Phi_{i,j} \in \{0, 1\}$. If it is possible to establish LOS links between nodes i and j, then $\Phi_{i,j} = \Phi_{j,i} = 1$. Otherwise, $\Phi_{i,j} = \Phi_{j,i} = 0$. In the considered FSO network, each node is equipped with one optical transceiver to transmit/receive its own traffic to the backbone node, which is equipped with N optical transceivers.

In order to take advantage of the cooperative reconfigurable FSO network, additional optical transceivers are implemented. For any w additional transceivers in the network, there are Λ possible transceiver placement vectors $Z_a = [z_k^a]$, where z_k^a is the total number of optical transceivers at the kth node, $k \in \{1, 2, \ldots, N\}$, for the ath placement vector, $a \in \{1, 2, \ldots, \Lambda\}$. Clearly, $z_k^a \in \{1, 2, \ldots, w+1\}$ and $w = \sum_{k=1}^{N} (z_k^a - 1)$. Also, the number of nodes equipped with s transceivers is given by n_s^a, where $s \in \{1, 2, \ldots, w+1\}$ and $N = \sum_{s=1}^{w+1} n_s^a$. Limiting $w \leq N$, all possible Z_a vectors can be summarized in a matrix H with dimension $\Lambda \times N$, and Λ is bounded by the following inequality:

$$\Lambda < \left[\binom{N}{1} + \sum_{b=2}^{w-1} \binom{N}{b} \times (w-1)^b + \binom{N}{w} \right], \quad w \leq N.$$

(9)

In this upper bound, the first N vectors could be generated by different combinations of one node (out of N FSO nodes) equipped by w transceivers. The second term represents a combination of b, $2 \leq b \leq w - 1$, nodes (out of N FSO nodes)

that could be equipped by w transceivers with all permutations of distributions, $(w-1)^b$. The reset of vectors could be produced by different alternatives for w out of N FSO nodes. Figure 2 shows two possible transceiver placements for a network that has $N = 9$ and $w = 4$. Figure 2(A) represents $Z_1 = (2, 2, 1, 2, 2, 1, 1, 1, 1)$, $n_1^1 = 5$, and $n_2^1 = 4$, while Fig. 2(B) represents $Z_2 = (3, 2, 1, 2, 1, 1, 1, 1, 1)$, $n_1^2 = 6$, $n_2^2 = 2$, and $n_3^2 = 1$.

The losses of all FSO links are summarized in an $(N+1) \times (N+1) \gamma = [\gamma_{i,j}]$ matrix, where $\gamma_{i,j}$ is the loss coefficient of the link between the transmitter of the ith node and the receiver of the jth node. Clearly for any $i, j \in \{0, 1, \ldots, N\}$, $0 \leq \gamma_{i,j} \leq 1$, $\gamma_{i,i} = 0$, and $\gamma_{i,j} = \gamma_{j,i}$.

It should be noted that for each transceiver placement vector $Z_a \in H$, there is a number of feasible configurations β_a that could be realized by this placement. All associated configurations with Z_a could be summarized in a connections matrix $G_a = [g_{i,j,d}^a]$ with dimension $(N+1) \times (N+1) \times \beta_a$, where $g_{i,j,d}^a \in \{0, 1\}$ is the connection status between the ith and jth nodes in configuration $d \in \{1, 2, \ldots, \beta_a\}$. The connection between nodes i and j is established in configuration d if $g_{i,j,d}^a \geq 1$. Clearly, if there is no LOS connection between nodes i and j, i.e., $\Phi_{i,j} = 0$, then $g_{i,j,d}^a = 0$. The upper bound of β_a could be obtained from the symmetry $g_{i,j,d}^a = g_{j,i,d}^a$ and zero diagonal $g_{i,j,d}^a = 0 d$th connection matrix. The first row of the upper triangle of this matrix represents all connections to/from a backbone node with different $\sum_{k=1}^{N} (N-k+1)^k \binom{N}{k}$ combinations. The next n_1^a rows of the triangle represent the connections to/from all nodes that have one transceiver, resulting in $\prod_{ii=1}^{n_1^a} \sum_{kk=0}^{1} \binom{N-ii}{kk}$ different connections. The next n_2^a rows of the triangle represent the connections to/from all nodes that have two transceivers, resulting in $\prod_{ii=1}^{n_2^a} \sum_{kk=0}^{2} \binom{N-ii-n_1^a}{kk}$ different connections, and so on. Therefore, β_a is upper bounded by

$$\beta_a < \sum_{k=1}^{N} \frac{\binom{N}{k}}{(N-k+1)^{-k}} \prod_{s=1}^{w+1} \prod_{ii=1}^{n_s^a} \sum_{kk=0}^{s} \binom{N-ii-\sum_{jj=1}^{s-1} n_{jj}^a}{kk}.$$

(10)

At a given Z_a, all FSO links are assumed to have adaptive average transmitted power, i.e., the power of the optical link between nodes i and j in configuration d is one of discrete values $p_{i,j,d}^a \in \{0, y_1, y_2, \ldots, y_Y\}$, where $y_1 < y_2 < \cdots < y_Y$. The average transmitted power of node k in configuration d is $p_{k,d}^a = \sum_{j=0}^{N} p_{k,j,d}^a$. However, to increase link capacity and guarantee an error rate $e_{i,j,d}^a$ less than a specified maximum BER $\text{BER}_{\max}$, the link between nodes i and j in configuration d adapts its transmission rate $t_{i,j,d}^a$ to be one of discrete values, i.e., $t_{i,j,d}^a \in \{0, x_1, x_2, \ldots, x_X\}$, where $x_1 < x_2 < \cdots < x_X$. The transmission rate of node k in configuration d is denoted by $t_{k,d}^a$, where $t_{k,d}^a = \sum_{j=0}^{N} t_{k,j,d}^a$. The bit rate of node k (its own traffic) through connection to node j in configuration d is denoted by $r_{k,j,d}^a$. The overall bit rate of node k in configuration d is $r_{k,d}^a = \sum_{j=0}^{N} r_{k,j,d}^a$.

Obviously, $r_{k,d}^a \le t_{k,d}^a$, and for practical implementation, both $r_{k,d}^a$ and $t_{k,d}^a \in \{0, x_1, x_2, \ldots, x_X\}$. The end-to-end BER of the kth node $e_{k,d}^a$ is bounded by $e_{k,j,d}^a \le e_{k,d}^a \le \mathrm{BER}_{\max}$. The bit rates and BERs associated with all nodes in the feasible configurations of Z_a could be summarized in $N \times \beta_a$ matrices $R_a = [r_{k,d}^a]$ and $E_a = [e_{k,d}^a]$, respectively.

The network capacity and average transmitted power associated with configuration d are given by $c_d^a = \sum_{k=1}^N r_{k,d}^a$ and $p_d^a = \sum_{k=1}^N p_{k,d}^a$, respectively. Also, all capacity and power values associated with all feasible configurations are summarized in vectors $C_a = [c_d^a]$ and $P_a = [p_d^a]$, with dimension $1 \times \beta_a$.

Network parameters:

H:	Feasible configuration matrix $\Lambda \times N$
γ:	Loss coefficient matrix $(N+1) \times (N+1)$
G_a:	Configurations matrix $(N+1) \times (N+1) \times \beta_a$
$t_{i,j,d}^a$:	Transmission rate between links i and j in the dth configuration
$t_{k,d}^a$:	Transmission rate of the kth node in the dth configuration
$r_{i,j,d}^a$:	Bit rate of the ith node to links i and j in the dth configuration
$r_{k,d}^a$:	Bit rate of the kth node in the dth configuration
R_a:	Bit rate matrix $\beta_a \times N$
$e_{i,j,d}^a$:	BER in link $i-j$ in the dth configuration
$e_{k,d}^a$:	BER of the kth node in the dth configuration
E_a:	BER matrix $\beta_a \times N$
$\mathrm{BER}_{\max}$:	BER threshold
$p_{i,j,d}^a$:	Average optical power of links i and j in the dth configuration
$p_{k,d}^a$:	Average optical power of the kth node in the dth configuration
P_a:	Power vector $\beta_a \times 1$
c_d^a:	Capacity of the dth configuration in the ath placement vector
C_a:	Capacity vector $\beta_a \times 1$
z_k^a:	Number of transceivers on the kth node
Z_a:	ath placement vector
w:	Additional number of transceivers in the network

4. PROPOSED OPTIMAL FSO TRANSCEIVER PLACEMENT SCHEMES

In cooperative dynamic FSO networks, in severe weather conditions, far FSO nodes connect to close ones in order to keep backhaul transmissions at one of the allowable discrete rates that guarantee BERs less than a certain threshold. In mobile networks, the network reliability metric is an important objective because it can represent both the fairness and capacity of the networks. It is also of growing interest because any failure of FSO nodes may lead to discounting the services for users in related areas, resulting in significant loss in both data and revenue [45]. Therefore, the first priority objective in cooperative dynamic FSO networks is to increase network reliability in terms of minimizing the number of dropped nodes under severe weather conditions. Moreover, given the placement of FSO transceivers, optimal resource allocation schemes

could be implemented to efficiently allocate network resources among different nodes in various weather conditions. In other words, optimal resource allocation schemes are deployed to increase network reliability as a fundamental objective, then either raise fairness among different nodes or keep network capacity at high atmospheric degradations. Resource allocation relies on possibilities of network reconfiguration, and it yields remarkable improvement in the performance by selecting the best configurations in different weather conditions. Clearly, as indicated by Eq. (10), these possibilities depend only on the number of placed FSO transceivers at each node. Thus, placement of FSO transceivers has a significant role and could be optimized in order to enhance the performance of resource allocation.

Transceiver placement and resource allocation schemes could be formulated to meet multiple objectives such as maximizing reliability, capacity, and fairness, and/or minimizing transmitted power and BERs. Clearly, raising network reliability implies decreasing the number of dropped nodes; increasing network capacity is achieved by maintaining the largest number of direct links to the central node, while enhancing fairness means nearly the same bit rates are assigned to connective nodes. In this section, two joint transceiver placement and resource allocation schemes are proposed, namely, maximum capacity optimal transceiver placement (MCOTP) and maximum fairness optimal transceiver placement (MFOTP). The schemes aim at obtaining optimal transceiver placements, based on the average performance of associated resource allocations in different weather conditions, in order to achieve the best average network performance for the given probability-distribution function (PDF) of visibility, rain, or/and snow droplet fall rates.

The dynamic FSO network performance obtained by any resource allocation scheme in the dth configuration associated with the Z_a placement vector could be presented by reliability $\Re_d^a$, network capacity C_d^a, fairness F_d^a, average transmitted power P_d^a, and average error rate ξ_d^a. Obviously, these metrics are obtained from network matrices and vectors R_a, C_a, P_a, and E_a, respectively. Network reliability $\Re_d^a$ of configuration d associated with transceiver placement a is computed from the number of active (non-dropped) nodes as

$$\Re_d^a = 1/N \times \sum_{k=1}^N \delta_{k,d}^a, \qquad \delta_{k,d}^a = \begin{cases} 1; & r_{k,d}^a > 0, \\ 0; & r_{k,d}^a = 0 \end{cases}, \quad \textbf{(11)}$$

where, $\delta_{k,d}^a$ is the node status coefficient. $\delta_{k,d}^a = 1$ if node k is active ($r_{k,d}^a > 0$), and $\delta_{k,d}^a = 0$ if node k is dropped ($r_{k,d}^a = 0$).

Also, the Jains index $0 \le F_d^a \le 1$ is used to evaluate fairness in assigned bit rates among surviving nodes [46]:

$$F_d^a = \left(\sum_{k=1}^{N \times \Re_d^a} r_{k,d}^a \right)^2 \Bigg/ \left(N \times \Re_d^a \times \sum_{k=1}^{N \times \Re_d^a} (r_{k,d}^a)^2 \right). \quad \textbf{(12)}$$

The average BER is computed as

$$\xi_d^a = \frac{1}{c_d^a} \sum_{k=1}^N r_{k,d}^a \times e_{k,d}^a. \quad \textbf{(13)}$$

Generally, the above metrics (objectives) conflict, and optimal values (global maximum or minimum) for these objectives cannot be achieved using one configuration. Thus, multi-objective optimization is used to formulate the proposed schemes. Particularly, lexicographic representations are addressed, in which objective functions are arranged in order of importance, then the objectives are optimized (maximized or minimized) one by one sequentially [47]. In this formulation, the MCOTP scheme sequentially optimizes reliability, capacity, average transmitted power, and average error rate. On the other side, MFOTP ignores capacity optimization and sequentially optimizes reliability, fairness, average transmitted power, and average error rate. Clearly, this enables the MFOTP scheme to achieve higher fairness levels than those of the MCOTP scheme. However, this comes with the price of reducing network capacity.

Naturally, the FSO link is a quasi-static channel, so it can maintain its performance for an interval of weather conditions [37]. Also, at a given transceiver placement vector Z_a, $a \in \{1, 2, \ldots, \Lambda\}$, and a specific value of visibility, there is an optimal network configuration that achieves the highest performance. However, a small change in visibility around this value will result in the same optimal configuration: no network reconfiguration if there are non-effective weather changes. However, the loss intervals associated with each transceiver placement vector Z_a are identified by numerical evaluations, and it depends on optimization formulation, geographical distribution of FSO nodes, and given transceiver placement. Clearly, this means that for each placement vector Z_a, there is a set of M_a optimal configurations associated with M_a visibility intervals that cover the entire range of visibility. These intervals could be presented using loss intervals $\Delta\gamma_{a,m}$, $m \in \{1, 2, 3, \ldots, M_a\}$, with known PDF $\Pr(\Delta\gamma_{a,m})$. The optimal configurations associated with placement vector Z_a are presented in matrix ${}^*G_a = [{}^*g^a_{i,j,m}]$ with dimension $(N+1) \times (N+1) \times M_a$. Clearly, the associated optimized bit rate and error rate matrices are ${}^*R_a = [{}^*r^a_{k,m}]$ and ${}^*E_a = [{}^*e^a_{k,m}]$, respectively, each with dimension $N \times M_a$. Also, the associated capacities, average powers, reliabilities, and fairnesses are listed in vectors ${}^*C_a = [{}^*c^a_m]$, ${}^*P_a = [{}^*p^a_m]$, ${}^*\Re^a = [{}^*\Re^a_m]$, and ${}^*F^a = [{}^*F^a_m]$, respectively, each with dimension $1 \times M_a$.

Among all feasible placement vectors listed in matrix H, there is an optimal placement vector Z_{a*} that achieves the highest constrained average network performance over the entire visibility range. Clearly, toward obtaining this optimal placement vector along with the associated optimal network configurations, two optimization steps are performed (bi-level optimization). In the first step, for each placement vector Z_a, optimal configuration matrices that optimize certain resource allocation ${}^*G_a$ along with associated loss interval $\Delta\gamma_{a,m}$ objectives are obtained. In the second step of the optimization, the optimal placement vector $Z_{a*} \in H$ that achieves the highest average performance along the entire atmospheric loss range is obtained. The following subsections formulate the two proposed joint placement and resource allocation schemes and show the flowchart that describes them.

A. Maximum-Capacity Optimal Transceiver Placement Scheme

The MCOTP scheme intends to optimize four performance objectives. The scheme maximizes or minimizes them sequentially based on the importance of each one. The MCOTP scheme prioritizes network reliability as the highest priority objective (essential objective of the dynamic FSO network), then capacity, average transmitted power, and average error rate in descending optimization order. The scheme is formulated in two optimization steps. In the first step, among all feasible β_a configurations associated with placement vector Z_a, the scheme obtains optimal M_a configurations (listed in the ${}^*G_a$ matrix) along with their associated loss intervals $\Delta\gamma_{a,m}$. In the second step, the scheme determines optimal placement vector Z_{a*} from all Λ feasible placement vectors that achieve the highest average performance over the entire visibility range. The steps are formulated using bi-level lexicographic optimization as the following:

Step One: Obtaining Optimal Configurations ${}^*G_a$ for Each Z_a.

<u>**Given**</u> : $\varsigma, Z_a, \beta_a, \gamma, a \in \{1, 2, 3, \ldots, \Lambda\}$.

$$\mathbf{Max}_d : \Re^a_d = 1/N \times \sum_{k=1}^{N} \delta^a_{k,d},$$

$$\mathbf{Max}_d : \left\{ c^a_d = \sum_{k=1}^{N} r^a_{k,d} : \Re^a_d = {}^* \Re^a_d \right\},$$

$$\mathbf{Min}_d : \left\{ p^a_d = \sum_{k=1}^{N} p^a_{k,d} : c^a_d = {}^* c^a_d \right\},$$

$$\mathbf{Min}_d : \xi^a_d = \frac{1}{c^a_d} \sum_{k=1}^{N} r^a_{k,d} \times e^a_{k,d} : p^a_d = {}^* p^a_d$$

$$d \in \{1, 2, 3, \ldots, \beta_a\},$$

Subject to:

$$\delta^a_{k,d} = \begin{cases} 1; & r^a_{k,d} > 0 \\ 0; & r^a_{k,d} = 0 \end{cases},$$

$$r^a_{k,d} = \sum_{i=0}^{N} r^a_{i,k,d}, \qquad t^a_{k,d} = \sum_{i=0}^{N} t^a_{i,k,d},$$

$$r^a_{k,d} \le t^a_{k,d}, \qquad e^a_{i,k,d} \le e^a_{k,d} \le \mathrm{BER}_{\max},$$

$$r^a_{k,d}, \quad r^a_{i,j,d}, \quad t^a_{k,d}, \quad t^a_{i,j,d} \in \{0, x_1, \ldots, x_X\},$$

$$p^a_{k,d} = \sum_{i=0}^{N} p^a_{i,k,d}, \qquad p^a_{i,j,d} \in \{0, y_1, y_2, \ldots, y_Y\},$$

$$i, j \in \{0, 1, 2, \ldots, N\}, \qquad j \ne i, \qquad k \in \{1, 2, \ldots, N\}.$$

<u>**Outputs**</u> : ${}^*G_a, {}^*C_a, {}^*R_a, {}^*P_a, {}^*E_a, \Delta\gamma_{a,m}, M_a.$

Step Two: Obtaining Optimal Placement Vector Z_{a*}

<u>**Given**</u> $: {}^{*}G_a, {}^{*}C_a, {}^{*}R_a, {}^{*}P_a, {}^{*}E_a, \Delta\gamma_{a,m}, M_a, \Pr(\Delta\gamma_{a,m})$.

$$\underset{a}{\textbf{Max}} : \left\{ \Omega_a^{\Re} = \sum_{m=1}^{M_a} \Pr(\Delta\gamma_{a,m}) \Delta\gamma_{a,m} \times {}^{*}\Re_m^a \right\},$$

$$\underset{a}{\textbf{Max}} : \left\{ \Omega_a^{c} = \sum_{m=1}^{M_a} \Pr(\Delta\gamma_{a,m}) \Delta\gamma_{a,m} \times {}^{*}c_m^a : \Omega_a^{\Re} = {}^{*}\Omega_a^{\Re} \right\},$$

$$\underset{a}{\textbf{Min}} : \left\{ \Omega_a^{p} = \sum_{m=1}^{M_a} \Pr(\Delta\gamma_{a,m}) \Delta\gamma_{a,m} \times {}^{*}P_m^a : \Omega_a^{c} = {}^{*}\Omega_a^{c} \right\},$$

$$\underset{a}{\textbf{Min}} : \left\{ \Omega_a^{\xi} = \sum_{m=1}^{M_a} \Pr(\Delta\gamma_{a,m}) \Delta\gamma_{a,m} \times {}^{*}\xi_m^a : \Omega_a^{p} = {}^{*}\Omega_a^{p} \right\},$$

$$a \in \{1, 2, 3, \ldots, \Lambda\}.$$

<u>**Outputs**</u> $: Z_{a*}, {}^{*}G_{a*}.$ (14)

In the first optimization step, for each transceiver placement vector Z_a and weather condition (such as visibility value V), the scheme finds first the configurations that maximize network reliability, i.e., the ones that have the maximum value in reliability vector $\Re^a$ among all feasible configurations listed in G_a. However, if there is more than one configuration that has the same maximum reliability, the scheme selects from them the ones that maximize network capacity. Moreover, if there is still more than one configuration that has the same maximum network capacity, the scheme selects from them the one that minimizes the average transmitted power in the network. Finally, if there is more than one configuration with the same average transmitted power, the scheme selects the one that achieves the minimum average BER in the network. Clearly, in this optimization step, network capacity is constrained by maximizing network reliability.

Several constraints are imposed in this step. The BER of each node must be less than a predefined threshold. Also, only specific discrete values for the bit rates, transmission rates, and transmitted optical power are allowed. Obviously, each optimal configuration is obtained at a specified visibility value. However, there is a range of visibility in which the obtained configuration has optimal performance. Thus, for each feasible placement vector Z_a, the outputs of the first optimization step are optimal M_a configurations (listed in the ${}^{*}G_a$ matrix) along with specified M_a loss intervals $\Delta\gamma_{a,m}$. Also, the associated optimized matrices and vectors ${}^{*}R_a, {}^{*}E_a, {}^{*}C_a,$ and ${}^{*}P_a$ are further obtained.

In the second optimization step, the optimal placement vector Z_{a*} is obtained that achieves the highest average performance over the entire visibility range. Particularly, for each placement vector Z_a and using the PDF of associated atmospheric loss intervals $\Pr(\Delta\gamma_{a,m})$, the average performance is computed for four objectives. The PDF of loss intervals is known from the annual probability distribution of visibility in specific geographical areas [48]. Several measurements have

been carried out in different cities around the world to develop a PDF for fog attenuation, which is used to study and evaluate the performance of FSO systems [49–52]. Also, historical climate data can be accessed by using the websites of weather forecasting centers, such as [53] in Canada. First, among all feasible Λ placement vectors listed in matrix H, MCOTP selects the placement vector that results in the highest average reliability $\Omega_a^{\Re}$. However, if there is more than one placement vector that achieves the same maximum average reliability, the scheme selects among them the one with the highest average capacity Ω_a^{c}. If there is still more than one placement vector that has the same maximum average capacity and reliability, the scheme selects sequentially the one with the lowest average transmitted power Ω_a^{p}, then lowest average BER Ω_a^{ξ}. The result of this optimization step is the optimal placement vector Z_{a*} and its associated optimal configurations ${}^{*}G_{a*}$.

B. Maximum Fairness Optimal Transceiver Placement Scheme

Toward achieving higher reliability and fairness levels in the network, the capacity objective of MCOTP optimization is replaced by the fairness objective resulting in the MFOTP scheme. In other words, MFOTP aims to find the optimal placement vector Z_{a*} that enhances average network reliability then fairness (in terms of achieved bit rate for each node) regardless of capacity performance. Obviously, the MFOTP scheme achieves higher fairness levels than the MCOTP scheme in the same weather conditions. The fairness objective is formulated using lexicographic max-min optimization for bit rates of all nodes. The MFOTP scheme is formulated like the MCOTP scheme in two optimization steps as follows:

Step One: Obtaining Optimal Configurations ${}^{*}G_a$ for Each Z_a.

<u>**Given**</u> $: Z_a, \beta_a, \gamma, a \in \{1, 2, 3, \ldots, \Lambda\}.$

$$\underset{d}{\textbf{Max}} : \Re_d^a = 1/N \times \sum_{k=1}^{N} \delta_{k,d}^a,$$

$$\underset{d}{\textbf{Lex-Max-Min}} : f_d^a = [r_{1,d}^a, \ldots, r_{k,d}^a, \ldots, r_{N,d}^a] : \Re_d^a = {}^{*}\Re_d^a,$$

$$\underset{d}{\textbf{Min}} : \left\{ p_d^a = \sum_{k=1}^{N} p_{k,d}^a : f_d^a = {}^{*}f_d^a \right\},$$

$$\underset{d}{\textbf{Min}} : \xi_d^a = \frac{1}{c_d^a} \sum_{k=1}^{N} r_{k,d}^a \times e_{k,d}^a : p_d^a = {}^{*}p_d^a$$

$$d \in \{1, 2, 3, \ldots, \beta_a\},$$ (15)

Subject to:

$$\delta_{k,d}^{a} = \begin{cases} 1; & r_{k,d}^{a} > 0 \\ 0; & r_{k,d}^{a} = 0 \end{cases},$$

$$r_{k,d}^{a} = \sum_{i=0}^{N} r_{i,k,d}^{a}, \qquad t_{k,d}^{a} = \sum_{i=0}^{N} t_{i,k,d}^{a},$$

$$r_{k,d}^{a} \leq t_{k,d}^{a}, \qquad e_{i,k,d}^{a} \leq e_{k,d}^{a} \leq \text{BER}_{\max},$$

$$r_{k,d}^{a}, \quad r_{i,j,d}^{a}, \quad t_{k,d}^{a}, \quad t_{i,j,d}^{a} \in \{0, x_1, \dots, x_X\},$$

$$p_{k,d}^{a} = \sum_{i=0}^{N} p_{i,k,d}^{a}, \; p_{i,j,d}^{a} \in \{0, y_1, y_2, \dots, y_Y\},$$

$$i, j \in \{0, 1, 2, \dots, N\}, \qquad j \neq i, \qquad k \in \{1, 2, \dots, N\}.$$

<u>**Outputs**</u> $: {}^{*}G_a, {}^{*}C_a, {}^{*}R_a, {}^{*}P_a, {}^{*}E_a, \Delta\gamma_{a,m}, M_a.$

Step Two: Obtaining Optimal Placement Vector Z_{a^*}.

<u>**Given**</u> $: {}^{*}G_a, {}^{*}C_a, {}^{*}R_a, {}^{*}P_a, {}^{*}E_a, \Delta\gamma_{a,m}, M_a, \Pr(\Delta\gamma_{a,m}).$

$$\underset{a}{\textbf{Max}} : \left\{ \Omega_a^{\Re} = \sum_{m=1}^{M_a} \Pr(\Delta\gamma_{a,m}) \Delta\gamma_{a,m} \times {}^{*}\Re_m^a \right\},$$

$$\underset{a}{\textbf{Max}} : \left\{ \Omega_a^{f} = \sum_{m=1}^{M_a} \Pr(\Delta\gamma_{a,m}) \Delta\gamma_{a,m} \times {}^{*}F_m^a : \Omega_a^{\Re} = {}^{*}\Omega_a^{\Re} \right\},$$

$$\underset{a}{\textbf{Min}} : \left\{ \Omega_a^{p} = \sum_{m=1}^{M_a} \Pr(\Delta\gamma_{a,m}) \cdot \Delta\gamma_{a,m} \cdot {}^{*}P_m^a : \Omega_a^{f} = {}^{*}\Omega_a^{f} \right\},$$

$$\underset{a}{\textbf{Min}} : \left\{ \Omega_a^{\xi} = \sum_{m=1}^{M_a} \Pr(\Delta\gamma_{a,m}) \Delta\gamma_{a,m} \times {}^{*}\xi_m^a : \Omega_a^{p} = {}^{*}\Omega_a^{p} \right\},$$

$$a \in \{1, 2, 3, \dots, \Lambda\}.$$

<u>**Outputs**</u> $: Z_{a^*}, {}^{*}G_{a^*}.$ (16)

## 5. MCOTP AND MFOTP SCHEME COMPLEXITY

The formulations of the MCOTP and MFOTP schemes are classified as multiple objective-bilevel-integer linear programming (MO-BL-ILP) problems. These problems could be solved using an exhaustive search (ES) method to obtain the optimal solutions. In the ES method, all feasible configurations are first generated using the predefined constraints. Then, the configurations are evaluated for the prioritized objective functions to obtain the best solutions [54]. Scheme complexity could be calculated in terms of the Λ, β_a, N, M_a parameters as

$$\Gamma \approx O\left(\frac{N^2}{2} \sum_{a=1}^{\Lambda} \beta_a \times M_a + 4 \sum_{a=1}^{\Lambda} M_a \right). \quad (17)$$

In this equation, the first term represents the approximated complexity for obtaining the optimal configuration among

β_a configurations for each possible placement a (first step optimization). For each configuration associated with transceiver placement a, the schemes calculate bit rates (network reliability), transmitted powers, and BERs for all nodes in order to obtain optimal configurations ${}^{*}G_a$. The computation of BERs involves many multiplications that represent the most important factor in computing scheme complexity. The average number of multiplications used to calculate the BERs of all nodes in each configuration is $N^2/2$. These multiplications are computed for all loss intervals M_a. The second term represents the approximated complexity for obtaining the optimal placement a^* among all Λ feasible transceiver placements that achieves the highest average network performance over the entire M_a loss intervals (second step optimization). In this step, the average performance of four objectives is computed with equal complexity of M_a multiplications.

Clearly, at large values of N, Λ, β_a, and M_a, the formulated problems cannot be solved in real-time environments. Therefore, in practical scenarios, given the annual weather distribution in the network area, the algorithms are solved off-line to obtain the optimal placement and its associated optimal configurations. The resultant placement is deployed, and its associated configurations are listed and stored at the backbone node in a lookup table indexed by the loss intervals. The flowchart for real-time operation of the proposed joint placement and resource allocation schemes is indicated in Fig. 3. Initially, each node is equipped with the pre-computed optimal number of FSO transceivers (once forever). The operation of resource allocation requires that each node periodically estimates the atmospheric attenuation of its FSO links. Then, the estimated values from all nodes are forwarded to
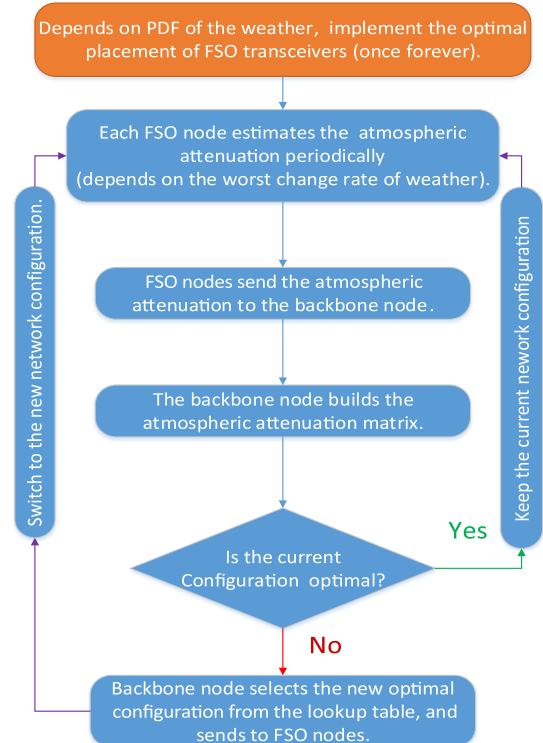
**Fig. 3.** Flowchart showing the real-time operation of the proposed schemes.
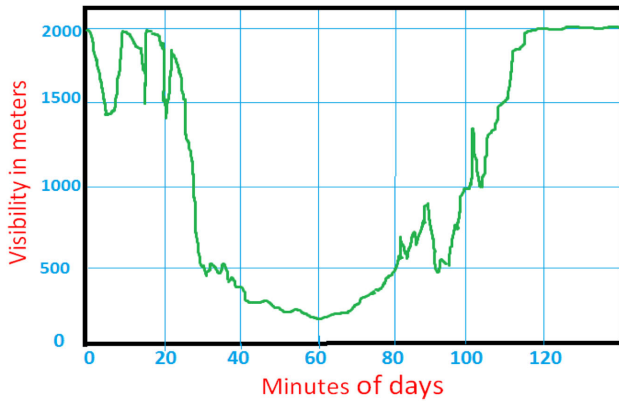
Fig. 4. Time series of a continental fog event recorded on 28 September 2007 at Prague (Czech Republic), according to [26].

Fig. 5. Considered geographical area of the FSO network.

the backbone node. Then, the backbone node indexes the stored lookup table by the received channel loss matrix and gets the corresponding optimal configuration. If the obtained configuration differs from the implemented one, the backbone node broadcasts the new configuration to all nodes. Otherwise, it keeps the current one.

The periodical time for channel estimation and network reconfiguration depends on the change rate of weather conditions. However, based on measured data of a continental fog event recorded at Prague and indicated in Fig. 4 [55], the fastest change rate of visibility is 3 m/s. On the other hand, as indicated in the simulations, the FSO network is reconfigured by changes larger than 200 m in visibility, and consequently, the reconfiguration time is selected to be less than 1 min. Furthermore, the FSO channel is classified as a quasi-static channel, and each optimal configuration is associated with an atmospheric attenuation range and not a specific value [55]. In a real-time sense, PAT switches FSO links (mechanically or electronically) among different stored configurations according to the atmospheric attenuation matrix.

6. SIMULATION AND NUMERICAL RESULTS

In this section, both the MCOTP and MFOTP schemes are numerically evaluated for two different values of additional transceivers $w \in \{3, 4\}$. The physical layout of the simulated network is indicated in Fig. 5, where nine FSO nodes are located uniformly in the network's area. Furthermore, the weather conditions of fog, rain, and snow rarely occur concurrently, and this enables the study of fog impact on network performance separately [5]. Also, visibility is assumed to be homogeneous throughout the service area. The simulation parameters are summarized in Table 1, where the maximum bit rate is 1 Gbps, minimum bit rate is 0.25 Gbps, maximum transmitted power is -15 dBm, minimum transmitted power is -18 dBm, and threshold BER is 10^{-4}. Also, the receiver diameter is assumed to be $d_r = 0.2$ m, and the largest computed FSO link distance is $L = 3700$ m. The aperture averaging is then calculated as $A = [1 + 1.33 \times (2\pi/\lambda \times d_r^2/L)]^{-7/5} = 0.0038$. Clearly, using this value of aperture averaging, the attenuation variance caused by weak turbulences has a small effect and can
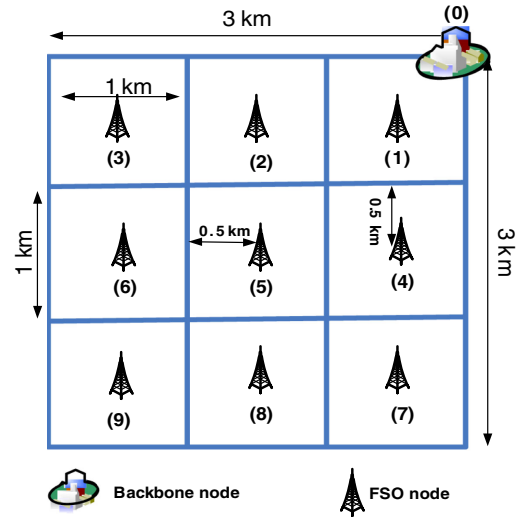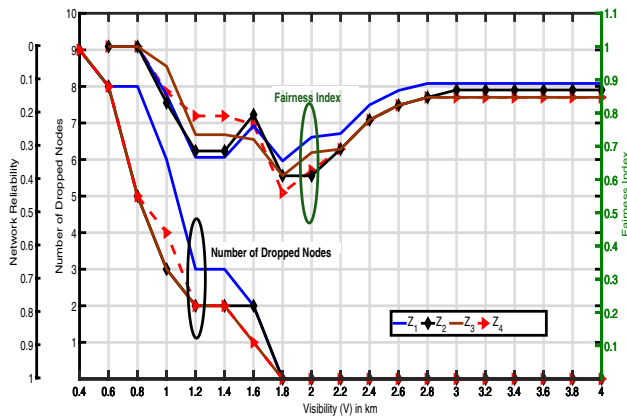
Table 1.   Simulation Parameters

Link Parameters	Values
Signal wavelength (λ)	1550 nm
Divergence angle (Θ)	2 mm · rad/m
Diameter of transmitter (d_t)	4 cm
Diameter of receiver (d_r)	20 cm
Average transmitted signal counts/slot	250,000
Average background counts/slot	50
Average transmitted power levels in dBm	$-(18, 17, 16.5, 16, 15)$
Average background noise power	-52 dBm
Discrete bit rates in Gbps	1, 3/4, 1/3, 1/2, 1/3, 1/4
Modulation formate	NR-OOK
BER threshold (BER$_{max}$)	10^{-4}
Area of FSO network	3×3 km^2
Area of FSO cell	1×1 km^2

be neglected [56]. Generally, including the fading caused by weak or strong scintillations will not change the problem formulation, and it could be added to other attenuations in the channel loss matrix γ.

Generally, to achieve higher performances in cooperative dynamic FSO networks, the additional FSO transceivers have to be installed at inner nodes (that have shorter distances to the center node) to enable them to act as relays for outer nodes. For the considered network with $\omega = 4$, the additional transceivers are distributed on nodes 1, 2, 4, and 5, which results in 29 different placements. However, to illustrate the performance difference of various transceiver placements, four placements $Z_1 = (1, 1, 1, 2, 4, 1, 1, 1, 1)$, $Z_2 = (2, 2, 1, 1, 3, 1, 1, 1, 1)$, $Z_3 = (4, 1, 1, 1, 2, 1, 1, 1, 1)$, and $Z_4 = (2, 2, 1, 2, 2, 1, 1, 1, 1)$ with $\omega = 4$ are semi-randomly selected and evaluated. Figures 6–8 demonstrate the performance of the MCOTP scheme at low visibilities. Figure 6 indicates both the number of dropped nodes (reliability) and the fairness versus visibility. Obviously, Z_3 achieves the highest reliability (lowest number of dropped nodes), while Z_1 gives the lowest one along all visibility ranges. Numerically at
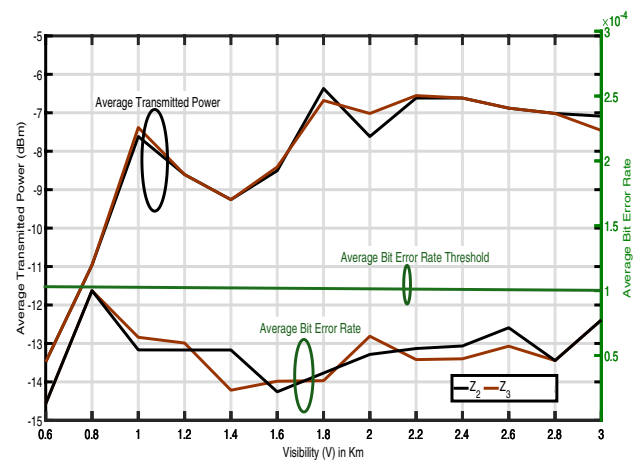
Fig. 6. Dropped nodes, reliability, and fairness performance of Z_1, Z_2, Z_3, and Z_4 versus visibility for the MCOTP scheme at $w = 4$.

Fig. 7. Network capacity of Z_1, Z_2, Z_3, and Z_4, along with optimal configurations of Z_3 versus visibility for the MCOTP scheme at $w = 4$.

Fig. 8. Average transmitted power and bit error rate for placements Z_2 and Z_3 versus visibility for the MCOTP scheme in the case of $w = 4$.
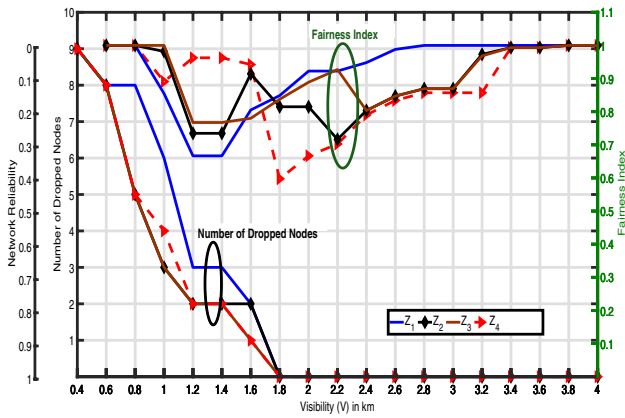
In this case, only one FSO link is used to connect node 1 to the central node with total system capacity of 1 Gbps, which is divided equally among the four active nodes.

In the same figure, the right y axis shows the index of optimal configurations for Z_3 versus visibility. However, this placement has 16 feasible configurations. For visibility range $V \geq 0.4$ km, the placement vector Z_3 has eight optimal network configurations with indices {2, 3, 4, 5, 6, 7, 10, 13}. For example, at 1.2 km $\leq V \leq 1.6$ km, the network configuration number 6 is the optimal one for MCOTP optimization and is presented by the following connection matrix:
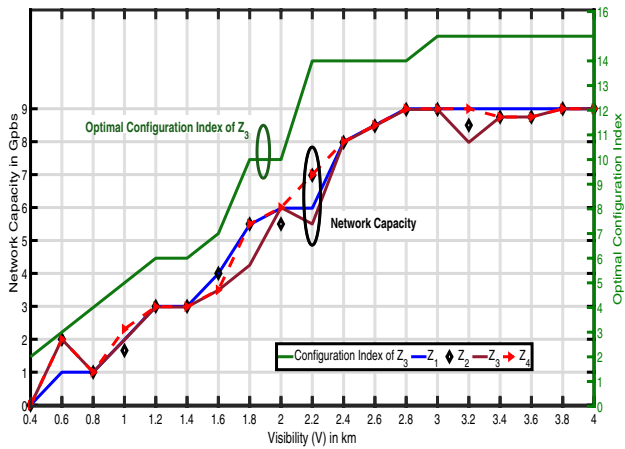
$$G_3|_6 = \begin{bmatrix} 0 & 2 & 1 & 0 & 1 & 1 & 0 & 0 & 1 & 1 \\ 2 & 0 & 0 & 1 & 0 & 0 & 0 & 1 & 0 & 0 \\ 1 & 0 & 0 & 0 & 0 & 0 & 0 & 0 & 0 & 0 \\ 0 & 1 & 0 & 0 & 0 & 0 & 0 & 0 & 0 & 0 \\ 1 & 0 & 0 & 0 & 0 & 0 & 0 & 0 & 0 & 0 \\ 1 & 0 & 0 & 0 & 0 & 0 & 1 & 0 & 0 & 0 \\ 0 & 0 & 0 & 0 & 0 & 1 & 0 & 0 & 0 & 0 \\ 0 & 1 & 0 & 0 & 0 & 0 & 0 & 0 & 0 & 0 \\ 1 & 0 & 0 & 0 & 0 & 0 & 0 & 0 & 0 & 0 \\ 1 & 0 & 0 & 0 & 0 & 0 & 0 & 0 & 0 & 0 \end{bmatrix}.$$

Clearly, the eight loss intervals associated with the optimal configurations of Z_3 are $\Delta\gamma_{3,1} = (0.4, 0.6)$, $\Delta\gamma_{3,2} = (0.6, 0.8)$, $\Delta\gamma_{3,3} = (0.8, 1)$, $\Delta\gamma_{3,4} = (1, 1.2)$, $\Delta\gamma_{3,5} = (1.2, 1.6)$, $\Delta\gamma_{3,6} = (1.6, 1.8)$, $\Delta\gamma_{3,7} = (1.8, 2.2)$, and $\Delta\gamma_{3,8} = (V \geq 2.2)$. Figure 8 shows the average transmitted power and average BER performance for placements Z_3 and Z_2. As shown, the error performance does not exceed the threshold 10^{-4} for the two placement vectors. Numerically, at $V = 2$ km, Z_3 costs transmitter power of -7 dBm to achieve a capacity of 6 Gbps, while Z_2 consumes -7.5 dBm and achieves 5.5 Gbps. Furthermore, at higher visibilities, the network consumes much less average power to maintain performance.

Figures 9 and 10 demonstrate the performance of the MFOTP scheme at different visibility values. Figure 9 shows an identical number of dropped nodes and reliability performance for the MCOTP scheme shown in Fig. 6 for the same placements Z_1, Z_2, Z_3, and Z_4. This is because both the MFOTP

$V = 1$ km, Z_1 has six dropped nodes (reliability of 0.33), and Z_4 has four dropped nodes (reliability of 0.54), while both Z_2 and Z_3 have three dropped nodes (reliability of 0.74). Also, as fairness optimization is not included explicitly in the formulation of MCOTP, the achieved fairness levels are relatively low. Numerically for $V \geq 2.8$ km, the fairness performances of Z_1, Z_2, Z_3, and Z_4 are 0.88, 0.86, 0.84, and 0.84, respectively.

Figure 7 shows the network capacity on the left y axis for the four placements. Obviously, all placements have nearly the same capacity values at higher visibilities, i.e., at $V \geq 2.2$ km. However, at low visibilities, different placements achieve different capacities. It is worth noting that the capacity of placement Z_3 is monotonically increased by increasing the visibility except at $V = 0.6$ km, as indicated in Fig. 7. At this value, only node 1 is active, and all other nodes are dropped, as indicated in Fig. 6. This node is connected to the central node using four FSO links, each with a capacity of 0.5 Gbps, resulting in total network capacity of 2 Gbps. However, at $V = 0.8$ km, the three additional transceivers existing on node 1 are used to connect it to nodes 2, 4, and 5, each with a capacity of 0.25 Gpbs.
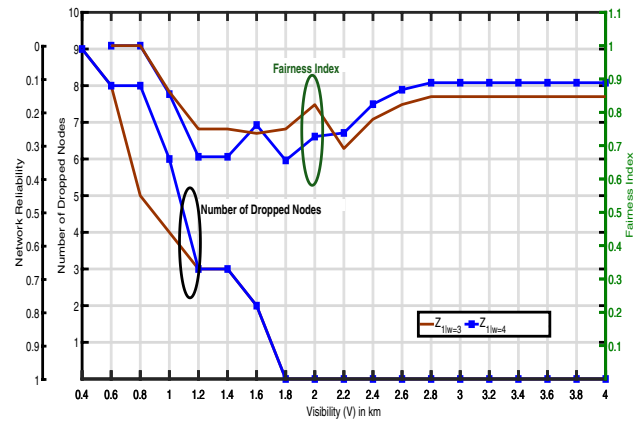
Fig. 9. Dropped nodes, reliability, and fairness performance of Z_1, Z_2, Z_3, and Z_4 versus visibility for the MFOTP scheme at $w = 4$.

Fig. 11. Network reliability, dropped nodes, and fairness performance of placements $Z_{1|w=3}$ and $Z_{1|w=4}$ versus visibility for MCOTP.

Fig. 10. Network capacity of Z_1, Z_2, Z_3, and Z_4 along with optimal configurations of Z_3 versus visibility for the MFOTP scheme at $w = 4$.

and MCOTP schemes have the maximization of network reliability as the first priority objective in their optimizations. However, the difference between the MFOTP and MCOTP schemes is in the achieved fairness and capacity performances. Clearly, Figs. 6 and 9 show that the fairness performance of the MFOTP scheme outperforms that of the MCOTP scheme. MFOTP achieves max-min fairness, which guarantees higher fairness among all nodes. Numerically, placements Z_1, Z_2, Z_3, and Z_4 gradually realize the maximum fairness of 1 at $V = 2.5, 3.4, 3.2$ and 3.4 km, respectively. Although Z_1 achieves the best fairness performance between surviving (connected) nodes, it has low reliability performance.

Figure 10 shows the network capacity performance for the four placements. Clearly, the capacities of all placements increase at higher visibilities. However, the capacity achieved by MCOTP is higher than that achieved by the MFOTP scheme, as indicated in Figs. 7 and 10. Numerically at $V = 2.2$ km, MCOTP realizes 7 Gbps by all placements, while MFOTP achieves 7, 7, 6, and 5.5 Gbps by Z_2, Z_4, Z_1, and Z_3, respectively. Also, Fig. 10 shows the indices

of optimal configurations associated with Z_3 versus visibility. Clearly, nine optimal configurations with indices $\{2, 3, 4, 5, 6, 7, 10, 14, 15\}$ out of 16 feasible ones are used to reconfigure the network for the entire visibility range. For example, at visibility ranges 2.2 km $\le V \le 3$ km and 3 km $\le V$, the best network configurations for optimal resource allocation are 14 and 15, respectively. In conclusion and according to Figs. 6–10, at $\omega = 4$, Z_3 presents the best placement vector among all possible vectors for both schemes.

Figures 11 and 12 show the performance achieved by using different numbers of redundant transceivers along with non-optimal placement. Specifically, the performances of two different placements, namely, $Z_{1|w=3} = (2, 2, 1, 1, 2, 1, 1, 1, 1)$ at $\omega = 3$ and $Z_{1|w=4} = (1, 1, 1, 2, 4, 1, 1, 1, 1)$ at $\omega = 4$, are compared for the MCOTP scheme. Figure 11 illustrates the network reliability and fairness performance for those placement vectors. Numerically, for 0.6 km $\le V \le 1.2$ km, $Z_{1|w=3}$ realizes higher network reliability and lower number of dropped nodes compared with $Z_{1|w=4}$. Also, for 1 km $\le V \le 2.2$ km, $Z_{1|w=3}$ achieves higher fairness performance than that of $Z_{1|w=4}$. However, at 1.4 km $\le V \le 2.2$ km, $Z_{1|w=4}$ achieves higher network capacity than that of $Z_{1|w=3}$, as indicated
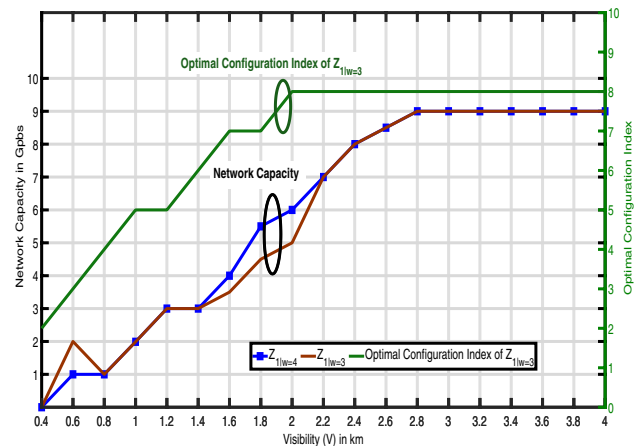
Fig. 12. Network capacity of $Z_{1|w=3}$ and $Z_{1|w=4}$ along with optimal configurations of $Z_{1|w=3}$ versus visibility for the MCOTP scheme.

in Fig. 12. As a result, a small number of optimally placed redundant transceivers can achieve better performance than that of many un-optimally placed ones. Thus, optimal transceiver placement plays an important role in the performance of cooperative dynamic FSO networks. Figure 12 shows the indices of optimal reconfiguration associated with $Z_{1|w=3}$ versus visibility. Along the entire visibility range, the placement vector $Z_{1|w=3}$ has seven optimal configurations with indices $\{2, 3, 4, 5, 6, 7, 8\}$, which achieve the best resource allocation for the MCOTP scheme.

7. CONCLUSION

Two joint placement and resource allocation schemes, MCOTP and MFOTP, are proposed to improve the average reliability and capacity or reliability and fairness performance of cooperative dynamic FSO networks, respectively. Each scheme is formulated as a MO-ML-ILP problem and is solved by the ES method to guarantee the optimality of the solution(s). Both schemes are evaluated and compared in foggy weather conditions. By using fewer optical transceivers, our results reveal that the proposed schemes achieve better average network reliability and bit rate fairness/capacity performance compared to random locations.

REFERENCES

1. I. I. Kim, B. McArthur, and E. J. Korevaar, "Comparison of laser beam propagation at 785 nm and 1550 nm in fog and haze for optical wireless communications," Proc. SPIE **4214**, 26–37 (2001).
2. H. H. Refai, J. J. Sluss, H. H. Refai, and M. Atiquzzaman, "Comparative study of the performance of analog fiber optic links versus free-space optical links," Opt. Eng. **45**, 025003 (2006).
3. S. Bloom, E. Korevaar, J. Schuster, and H. Willebrand, "Understanding the performance of free-space optics [Invited]," J. Opt. Netw. **2**, 178–200 (2003).
4. "Prediction methods required for the design of terrestrial free-space optical links," ITU-R Recommendation P.1814 (2007).
5. A. Vavoulas, H. G. Sandalidis, and D. Varoutas, "Weather effects on FSO network connectivity," J. Opt. Commun. Netw. **4**, 734–740 (2012).
6. N. Li and J. C. Hou, "Localized topology control algorithms for heterogeneous wireless networks," IEEE/ACM Trans. Netw. **13**, 1313–1324 (2005).
7. T. Shang, Y. Yang, G. Ren, B. Hu, T. Ding, and W. Chen, "Topology control algorithm and dynamic management scheme for mobile FSO networks," J. Opt. Commun. Netw. **7**, 906–917 (2015).
8. Y. Kaymak, R. Rojas-Cessa, J. Feng, N. Ansari, M. Zhou, and T. Zhang, "A survey on acquisition, tracking, and pointing mechanisms for mobile free-space optical communications," IEEE Commun. Surv. Tutorials **20**, 1104–1123 (2018).
9. C. Abou-Rjeily and W. Fawaz, "Buffer-aided serial relaying for FSO communications: asymptotic analysis and impact of relay placement," IEEE Trans. Wireless Commun. **17**, 8299–8313 (2018).
10. L. D. Truong, H. T. T. Pham, N. T. Dang, and T. V. Doan, "Topology design and cross-layer optimization for FSO mesh networks impaired by atmospheric turbulence and misalignment fading," J. Opt. Commun. Netw. **9**, 1097–1107 (2017).
11. Z. Hu, P. Verma, and J. Sluss, Jr., "Improved reliability of free-space optical mesh networks through topology design," J. Opt. Netw. **7**, 436–448 (2008).
12. M. A. Kashani, M. Safari, and M. Uysal, "Optimal relay placement and diversity analysis of relay-assisted free-space optical communication systems," J. Opt. Commun. Netw. **5**, 37–47 (2013).
13. B. Zhu, J. Cheng, and L. Wu, "Optimal FSO relay nodes placement with link obstacles and infeasible regions," in *Global Communications Conference (GLOBECOM)* (IEEE, 2014), pp. 2137–2142.
14. M. N. Smadi, S. C. Ghosh, A. A. Farid, T. D. Todd, and S. Hranilovic, "Free-space optical gateway placement in hybrid wireless mesh networks," J. Lightwave Technol. **27**, 2688–2697 (2009).
15. J. Yan, B. Zhu, G. Zhang, and J. Cheng, "Optimal user node placement for multi-hop FSO broadcasting communications under weak turbulence conditions," in *15th Canadian Workshop on Information Theory (CWIT)*, June 11, 2017, pp. 1–5.
16. S. D. Milner, T.-H. Ho, I. I. Smolyaninov, S. Trisno, and C. C. Davis, "Free-space optical wireless links with topology control," Proc. SPIE **4821**, 175–180 (2002).
17. A. S. Ghazy, H. A. I. Selmy, and H. M. H. Shalaby, "Fair resource allocation schemes for cooperative dynamic free-space optical networks," J. Opt. Commun. Netw. **8**, 822–834 (2016).
18. J. Tan, Y. Wang, M. Zhang, J. Liu, D. Liu, J. Tang, Z. Zhang, and N. Zhu, "All-optical transparent forwarding relay system for interstellar optical communication networks," IEEE J. Quantum Electron. **54**, 1–7 (2018).
19. A. S. Ghazy, H. A. I. Selmy, and H. M. H. Shalaby, "Fair cooperative resource allocation schemes for foggy free space optical network," in *17th International Conference on Transparent Optical Networks (ICTON)*, July 5, 2015, pp. 1–5.
20. A. S. Ghazy, H. A. I. Selmy, and H. M. H. Shalaby, "Reliable-fair resource allocation schemes for snowy free space optical (FSO) networks," in *Asia Communications and Photonics Conference* (Optical Society of America, 2015), paper ASu1H.4.
21. S. Song, Y. Liu, L. Guo, Y. Meng, and N. Lu, "Power allocation for maximum effective transmission in cooperative FSO networks," in *Asia Communications and Photonics Conference (ACP)*, October 26, 2018, pp. 1–3.
22. F. Ahdi and S. Subramaniam, "Optimal placement of FSO relays for network disaster recovery," in *IEEE International Conference on Communications (ICC)* (IEEE, 2013), pp. 3921–3926.
23. A. S. Ghazy, H. A. I. Selmy, Z. A. El-Sahn, and H. M. H. Shalaby, "Constrained fairness placement scheme in cooperative dynamic free space optical network," in *18th International Conference on Transparent Optical Networks (ICTON)*, July 10, 2016, pp. 1–5.
24. A. S. Ghazy, H. A. I. Selmy, and H. M. H. Shalaby, "Fair optimal transceivers placement in foggy cooperative dynamic FSO networks," in *Asia Communications and Photonics Conference* (Optical Society of America, 2016), paper AF2A.142.
25. Z. Gu, J. Zhang, and Y. Ji, "Topology optimization for FSO-based fronthaul/backhaul in 5G+ wireless networks," in *IEEE International Conference on Communications Workshops (ICC Workshops)*, May 20, 2018, pp. 1–6.
26. B. Makki, T. Svensson, M. Brandt-Pearce, and M. Alouini, "Performance analysis of RF-FSO multi-hop networks," in *IEEE Wireless Communications and Networking Conference (WCNC)*, March 19, 2017, pp. 1–6.
27. B. Makki, T. Svensson, M. B. Pearce, and M. Alouini, "On the performance of millimeter wave-based RF-FSO multi-hop and mesh networks," IEEE Trans. Wireless Commun. **16**, 7746–7759 (2017).
28. M. A. Hasabelnaby, H. A. I. Selmy, and M. I. Dessouky, "Joint optimal transceiver placement and resource allocation schemes for redirected cooperative hybrid FSO/mmw 5G fronthaul networks," J. Opt. Commun. Netw. **10**, 975–990 (2018).
29. F. Ahdi and S. Subramaniam, "Optimal placement of FSO links in hybrid wireless optical networks," in *IEEE Global Telecommunications Conference (GLOBECOM)*, December 5, 2011, pp. 1–6.
30. Y. Tang and M. Brandt-Pearce, "Link allocation, routing, and scheduling for hybrid FSO/RF wireless mesh networks," J. Opt. Commun. Netw. **6**, 86–95 (2014).
31. M. A. Hasabelnaby, H. A. I. Selmy, M. Dessoky, and A. Srivastava, "Performance enhancement of relayed hybrid FSO/MMW fronthaul network in C-RAN architecture," in *20th International Conference on Transparent Optical Networks (ICTON)*, July 1, 2018, pp. 1–4.
32. P. Pesek, S. Zvánovec, P. Chvojka, Z. Ghassemlooy, and P. A. Haigh, "Demonstration of a hybrid FSO/VLC link for the last mile and last meter networks," IEEE Photon. J. **11**, 1–7 (2019).

33. A. Gupta, N. Sharma, P. Garg, and M. Alouini, "Cascaded FSO-VLC communication system," IEEE Wireless Commun. Lett. **6**, 810–813 (2017).

34. M. Li and M. Cvijetic, "Coherent free space optics communications over the maritime atmosphere with use of adaptive optics for beam wavefront correction," Appl. Opt. **54**, 1453–1462 (2015).

35. M. Li, M. Cvijetic, Y. Takashima, and Z. Yu, "Evaluation of channel capacities of OAM-based FSO link with real-time wavefront correction by adaptive optics," Opt. Express **22**, 31337–31346 (2014).

36. M. Li, W. Gao, and M. Cvijetic, "Slant-path coherent free space optical communications over the maritime and terrestrial atmospheres with the use of adaptive optics for beam wavefront correction," Appl. Opt. **56**, 284–297 (2017).

37. M. A. Khalighi and M. Uysal, "Survey on free space optical communication: a communication theory perspective," IEEE Commun. Surv. Tutorials **16**, 2231–2258 (2014).

38. M. A. Esmail, H. Fathallah, and M. Alouini, "Outdoor FSO communications under fog: attenuation modeling and performance evaluation," IEEE Photon. J. **8**, 1–22 (2016).

39. A. Kaur and M. L. Singh, "Performance evaluation of free space optics (FSO) and radio frequency communication system due to combined effect of fog and snow," in IJCA Proceedings on International Conference on Recent Advances and Future Trends in Information Technology (iRAFIT) (2012), pp. 32–36.

40. M. Uysal, C. Capsoni, Z. Ghassemlooy, A. Boucouvalas, and E. Udvary, Optical Wireless Communications: An Emerging Technology (Springer, 2006).

41. J. Sui, G. Koehler, and F. Krol, "Characteristics of rainfall, snowmelt and runoff in the headwater region of the main river watershed in germany," Water Res. Manage. **24**, 2167–2186 (2010).

42. "Propagation data required for the design of terrestrial free-space optical links," ITU-R Recommendation P.1817-1 (2012).

43. O. Barsimantov and V. V. Nikulin, "Adaptive optimization of a free space laser communication system under dynamic link attenuation," J. Opt. Commun. Netw. **3**, 215–222 (2011).

44. R. M. Gagliardi and S. Karp, Optical Communications, 2nd ed. (Wiley, 1995).

45. J. Zhang, K. Zhu, H. Zang, N. S. Matloff, and B. Mukherjee, "Availability-aware provisioning strategies for differentiated protection services in wavelength-convertible WDM mesh networks," IEEE/ACM Trans. Network. **15**, 1177–1190 (2007).

46. R. Jain, D. Chiu, and W. Hawe, "A quantitative measure of fairness and discrimination for resource allocation in shared computer systems," arXiv preprint cs/9809099 (1998).

47. R. T. Marler and J. S. Arora, "Survey of multi-objective optimization methods for engineering," Struct. Multidiscip. Optim. **26**, 369–395 (2004).

48. K. Wakamori, K. Kazaura, and I. Oka, "Experiment on regional broadband network using free-space-optical communication systems," J. Lightwave Technol. **25**, 3265–3273 (2007).

49. M. S. Khan, M. S. Awan, E. Leitgeb, F. Nadeem, and I. Hussain, "Selecting a distribution function for optical attenuation in dense continental fog conditions," in International Conference on Emerging Technologies, October 19, 2009, pp. 142–147.

50. M. A. Esmail, H. Fathallah, and M. Alouini, "Channel modeling and performance evaluation of FSO communication systems in fog," in 23rd International Conference on Telecommunications (ICT), May 16, 2016, pp. 1–5.

51. R. M. Chmielecki and A. E. Raftery, "Probabilistic visibility forecasting using Bayesian model averaging," Mon. Weather Rev. **139**, 1626–1636 (2011).

52. J. Ojo, O. Lawrence, and G. Ibitola, "Performance probability distribution function for modeling visibility for free space optical link in Nigeria," World Sci. News **109**, 211–234 (2018).

53. http://climate.weather.gc.ca/.

54. C. Paar and J. Pelzl, Understanding Cryptography: A Textbook for Students and Practitioners (Springer, 2009).

55. F. Nadeem, V. Kvicera, M. S. Awan, E. Leitgeb, S. S. Muhammad, and G. Kandus, "Weather effects on hybrid FSO/RF communication link," IEEE J. Sel. Areas Commun. **27**, 1687–1697 (2009).

56. L. C. Andrews, R. L. Phillips, and C. Y. Hopen, Laser Beam Scintillation with Applications (SPIE, 2001).

Abdallah S. Ghazy was born in Giza, Egypt, in 1983. He received a B.S. degree in electrical engineering from Azher University, Cairo, Egypt, in 2007. He received a M.Sc degree from the Egypt-Japan University of Science and Technology, Alexandria, Egypt, in 2016. He is currently working toward a Ph.D. degree at McMster University, Hamilton, Ontario, Canada. His research interests include optical communications, wireless communications, and heterogeneous communications networks.

Mahmoud A. Hasabelnaby was born in Menouf, Egypt, in 1992. He received B.S. (Hons.) and M.S. degrees in electrical engineering from Menoufia University, Menouf, Egypt, in 2014 and 2019, respectively. He is currently working toward a Ph.D. degree at the University of British Columbia, Okanagan Campus, Kelowna, Canada. His research interests include optical communications, wireless communications, heterogeneous communications networks, and next-generation wireless access networks.

Hossam A. I. Selmy was born in Giza, Egypt, in 1979. He received B.S. and M.S. degrees from Cairo University, Cairo, Egypt, in 2001 and 2007, respectively, and a Ph.D. degree from the Egypt-Japan University for Science and Technology, Alexandria, Egypt, in 2013, all in electrical engineering. He is currently an Associate Professor at the National Institute of Laser Enhanced Science (NILES), Cairo University, Cairo, Egypt. His research interests include advanced modulation and multiple access schemes for optical fiber communication and next-generation wireless access networks.

Hossam M. H. Shalaby was born in Giza, Egypt, in 1961. He received B.S. and M.S. degrees from Alexandria University, Alexandria, Egypt, in 1983 and 1986, respectively, and a Ph.D. degree from the University of Maryland at College Park in 1991, all in electrical engineering. In 1991, he joined the Electrical Engineering Department, Alexandria University, and was promoted to Professor in 2001. From September 2010 to August 2016, he was the Chair of the Department of Electronics and Communications Engineering, Egypt-Japan University of Science and Technology (E-JUST), Alexandria, Egypt. From September 1996 to January 1998, he was with the Electrical and Computer Engineering Department, International Islamic University Malaysia, and from February 1998 to February 2001, he was with the School of Electrical and Electronic Engineering, Nanyang Technological University, Singapore. His research interests include optical communication, silicon photonics, optical space division multiplexing, optical CDMA, and information theory. He is a senior member of the IEEE Photonics Society and The Optical Society (OSA).